Macromolecules
ARTICLE

Macromolecules **2009**, *42*, 5605–5613 **5605**
DOI: 10.1021/ma9008115

Multicompartment Nanoparticles Formed by a Heparin-Mimicking Block Terpolymer in Aqueous Solutions

Mariusz Uchman,* Miroslav Štěpánek, and Karel Procházka

Department of Physical and Macromolecular Chemistry, Faculty of Science, Charles University in Prague, Hlavova 2030, 12840 Prague 2, Czech Republic

Grigoris Mountrichas and Stergios Pispas*

Institute of Theoretical & Physical Chemistry, National Hellenic Research Foundation, 48 Vass. Constantinou Ave., 11635 Athens, Greece

Ilja K. Voets

Laboratory of Physical Chemistry and Colloid Science, Wageningen University, Dreijenplein 6, 6703, HB, Wageningen, The Netherlands

Andreas Walther

Makromolekulare Chemie II and Bayreuther Zentrum für Kolloide und Grenzflächen, Universität Bayreuth, D-95440 Bayreuth, Germany

Received April 14, 2009; Revised Manuscript Received May 11, 2009

ABSTRACT: A new amphiphilic block terpolymer poly((sulfamate-carboxylate)isoprene)-*block*-polystyrene-*block*-poly(ethylene oxide), $PISC_{230}$-PS_{52}-PEO_{151}, with a narrow molecular weight distribution (PDI = 1.05), was synthesized via the post polymerization reaction of the anionically prepared precursor block terpolymer polyisoprene-*block*-polystyrene-*block*-poly(ethylene oxide) with chlorosulfonyl isocyanate. The formation and structure of self-assemblies of the polyelectrolyte block terpolymer in dilute aqueous solutions were studied by static and dynamic light scattering, atomic force and cryogenic transmission electron microscopy, fluorometry, and ^{1}H NMR spectroscopy. In acidic solutions, the terpolymers self-assemble into kinetically trapped multicompartment micelles, with the core consisting of discrete PS and PISC domains and PEO in the shell. If the solution pH is adjusted to the alkaline region, the multicompartment micelles undergo an irreversible transition to regular micelles, with a PS core and a mixed shell formed by PEO and PISC blocks.

Introduction

Amphiphilic block copolymer micelles consisting of two distinct, microphase-separated domains, an inner hydrophobic core, and an outer water-soluble shell, have been widely investigated.[1−4] In most cases, such micelles are formed by linear AB diblock or, less frequently, by ABA and BAB triblock copolymers, where A is a hydrophilic, shell-forming block and B a hydrophobic, core-forming block.

In recent years, self-assemblies formed by various multiblock copolymers have gained considerable research interest. The presence of more than two mutually incompatible blocks in the copolymer architecture leads to the formation of multicompartment micelles consisting of more then two domains.[5,6]

Different strategies can be applied for the preparation of multicompartment micelles. The simplest and most straightforward is the self-assembly of linear[7−12] or starlike[13−15] ABC block terpolymer, or multiblock copolymers such as ABCA[16] and ABCBA,[17] where A is a hydrophilic block and B and C are incompatible hydrophobic blocks. Another approach is based on blending two diblocks such as AB and BC[18−20] or terpolymers such as ABC and ABD[21] or starlike ABC triblocks with AB[22] copolymers. Dissimilar A and B or A, B, and C blocks arranged into a comb-like architecture usually do not associate and are frequently called unimolecular micelles.[23,24] Further possibilities to form multicompartment nanoparticles rise from noncovalent attractive interactions such as hydrogen bonding[19,25−28] or electrostatic attraction[29] between two different blocks. If the above-mentioned interactions act as the driving force for the micellization, the self-assembly can be tuned by changing solvent composition, pH, ionic strength, and so on. It is interesting that one can also comicellize two block copolymers having a common block, such as AB and BC diblocks and prepare micelles resembling those formed by the corresponding ABC terpolymer.[30−33] Regioselective cross-linking of the outer regions of the amphiphilic block copolymer micelles provides great opportunity to create a wide spectrum of multicompartment nanoparticles.[21,34−36]

Morphologies of micelles prepared by the above-mentioned procedures range from various spherical particles such as "onion",[30−33] "Janus",[29,37] and "raspberry-like"[7,12,38] micelles to cylinders,[10,14,20,21] helices,[34] and "donut-shaped"[36] particles. These complex micellar morphologies can find applications in drug delivery, biotechnology, lithography, and catalysis.[5,6]

*To whom correspondence should be addressed.
E-mail: mariuszuchman@go2.pl (M.U.); pispas@eie.gr (S.P.).

Published on Web 05/29/2009

Scheme 1. Ionic Forms of Poly((sulfamate-carboxylate)isoprene) in Aqueous Solution

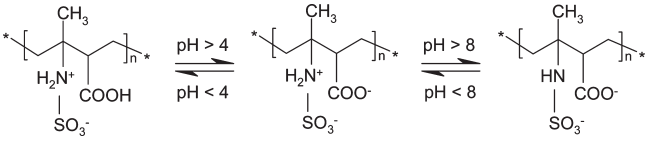

In this paper we describe the synthesis and self-assembly of a novel ABC linear block terpolymer consisting of a hydrophilic poly(ethylene oxide) (PEO) block, a short hydrophobic polystyrene (PS) middle block, and a poly((sulfamate-carboxylate)isoprene) (PISC) polyelectrolyte block. The latter is a biocompatible hydrophilic polymer that mimics the chemical structure of heparin.[39] It contains both strong (SO_3^-) and weak (NH_2^+, COO^-) electrolyte groups (Scheme 1). In aqueous solutions, PISC exists in different ionic forms depending on pH. It is noteworthy that heparin is widely used as an injectable anticoagulant and has the highest negative charge density of any known biological molecule.[40] Due to the presence of the PS block, the aqueous dispersions of $PISC_{230}$-PS_{52}-PEO_{151} nanoparticles were prepared indirectly using tetrahydrofuran (a good solvent for PS) as a cosolvent.

The structure of $PISC_{230}$-PS_{52}-PEO_{151} nanoparticles in aqueous solutions is studied at different pH by static and dynamic light scattering, atomic force microscopy, cryogenic transmission electron microscopy, and steady-state fluorometry with pyrene as a polarity-sensitive fluorescent probe.

Experimental Section

Materials. *Synthesis of the Terpolymer*. The synthesis of the terpolymer polyisoprene-*block*-polystyrene-*block*-poly(ethylene oxide) (PI_{230}-PS_{52}-PEO_{151}) precursor block terpolymer was carried out by living anionic polymerization employing high vacuum techniques.[41] First, isoprene was polymerized in benzene at room temperature, using *s*-butyl lithium as initiator. Subsequently, the second monomer styrene was added, together with a small amount of THF and the polymerization of the middle PS block occurred at room temperature. Finally, ethylene oxide and phosphazine base were added and the temperature of the reaction mixture was raised to 40 °C to affect preparation of the PEO block. The polymerization was terminated by addition of degassed methanol with two drops of concentrated HCl. At the end of each polymerization step, aliquots were isolated to control the success of the polymerization. The polyisoprene block of the precursor polymers was functionalized, as has been previously reported.[39] In particular, a predetermined amount of polymer was placed in a two-necked 100 mL round-bottom flask equipped with a septum. Carefully dried diethyl ether was distilled into the flask under vacuum, and the terpolymer was left to dissolve overnight (final terpolymer concentration was $c = 50$ g L^{-1}). Then, chlorosulfonyl isocyanate (CSI, from Acros) was added under N_2 dropwise, while the temperature was kept at 0 °C. The reaction of the polymer with CSI was continued for 6 h at 0 °C in the dark and under a stream of N_2. It has to be noted that precipitation was observed after 1 h of reaction. An amount of NaOH solution in water/methanol (1/3) was added dropwise. The diethyl ether was evaporated in vacuum and the remaining solution was refluxed overnight under N_2. After the end of the reaction the solvents were evaporated under vacuum and the solid was dialyzed against water.

Preparation of the Nanoparticles. Tetrahydrofuran (2 mL; THF, from Fluka, UV spectroscopy grade) was added to 20 mg of the sample, and the mixture was heated at 60 °C for about 1.5 h. Subsequently, 8 mL of aqueous 0.1 M HCl, was added dropwise under vigorous stirring, and the solution was heated at 60 °C for an additional 1.5 h. THF was then removed by dialysis of the solution against aqueous 0.1 M HCl. The final concentrations of $PISC_{230}$-PS_{52}-PEO_{151} nanoparticles in resulting aqueous solutions were about 2 g L^{-1}.

Techniques. *Size Exclusion Chromatography (SEC)*. The used SEC system consisted of a Waters 1515 pump, three μ-styragel separation columns with a continuous porosity of 10^2-10^5 Å, and a Waters 2414 differential refractive index detector. The solvent was tetrahydrofuran and the flow rate was 1 mL/min. The calibration of the instrument was performed using narrow polystyrene standards (M_w varying from 2500 to 900000).

NMR Spectroscopy. ^{1}H NMR spectra were recorded on a Varian 300 spectrometer at 25 °C. Solid state ^{13}C NMR spectra were recorded on a Bruker Avance 500 spectrometer at 25 °C.

Light Scattering Measurements. The light scattering setup (ALV, Langen, Germany) consisted of a 22 mW He−Ne laser, operating at the wavelength $\lambda = 632.8$ nm, an ALV CGS/8F goniometer, an ALV High QE APD detector, and an ALV 5000/EPP multibit, multitau autocorrelator. The solutions for measurements were filtered through 0.45 μm Acrodisc filters. The measurements were carried out for different concentrations (0.25−2.0 g L^{-1}) and different angles, θ, at 20 °C.

Static light scattering (SLS) measurements were treated by the Zimm method using the equation

$$\frac{Kc}{\Delta R_\theta(q,c)} = \frac{1}{\langle M\rangle_w}\left(1 + \frac{1}{3}\langle S^2\rangle_z q^2\right) + 2A_2 c \qquad (1)$$

where $\langle M\rangle_w$, $\langle S^2\rangle^{1/2}$, and A_2, respectively, are the weight-averaged molar mass, *z*-averaged radius of gyration, and the "light-scattering-averaged" osmotic second virial coefficient of the polymer in the solution, $\Delta R_\theta(q,c)$ is the corrected excess Rayleigh ratio that depends on the polymer concentration c and on the magnitude of the scattering vector $q = (4\pi n_0/\lambda)\sin(\theta/2)$. Here θ is the scattering angle, n_0 is the refractive index of the solvent, and λ is the wavelength of the incident light in vacuum. For light polarized perpendicularly to the plain of measurement, the contrast factor K is given by the relationship

$$K = \frac{4\pi^2 n_0^2}{\lambda^4 N_A}\left(\frac{dn}{dc}\right)^2 \qquad (2)$$

where (dn/dc) is the refractive index increment of the polymer with respect to the solvent and N_A is the Avogadro constant.

The refractive index increment of the $PISC_{230}$-PS_{52}-PEO_{151} terpolymer was calculated on the basis of terpolymer compositions as the weighted average of the literature values for PS and PEO ($(dn/dc)_{PS} = 0.257$, $(dn/dc)_{PEO} = 0.130$)[42] and the value for PISC obtained by the measurement with the Brice−Phoenix differential refractometer. The latter was measured as a function of pH under the conditions of osmotic equilibrium between the homopolymer solution and the solvent. The values of the terpolymer refractive index increments in studied aqueous solutions are as follows: 0.165 mL g^{-1} in 0.1 M HCl, 0.171 mL g^{-1} in H_2O, and 0.176 mL g^{-1} in 0.05 M $Na_2B_4O_7$.

Dynamic light scattering measurements were evaluated by fitting of the measured normalized time autocorrelation function of the scattered light intensity, $g^{(2)}(t)$, related to the electric field time autocorrelation function, $g^{(1)}(t)$, by the Siegert equation

$$g^{(2)}(t) = 1 + \beta|g^{(1)}(t)|^2 \qquad (3)$$

where t is the lag time and β is the coherence factor accounting for the deviation from the ideal correlation. The $g^{(1)}(t)$ function was fitted to the second order cumulant expansion

$$\ln g^{(1)}(t) = -\Gamma_1 t + \frac{1}{2}\Gamma_2 t^2 \qquad (4)$$

where Γ_1 and Γ_2, respectively, are the first and the second moment of the distribution function of relaxation rates. The Γ_1/q^2 values obtained from the fits of autocorrelation functions obtained at different scattering angles and terpolymer concentrations were further extrapolated to zero q and c to yield the z-averaged diffusion coefficient of the particles, $\langle D\rangle_z$, using the relationship

$$\frac{\Gamma_1(q,c)}{q^2} = \langle D\rangle_z(1 + k_D c + C\langle S^2\rangle_z q^2) \quad (5)$$

where k_D is the hydrodynamic virial coefficient and C is a coefficient determined by the slowest internal motion and polydispersity of the scattering particles. The hydrodynamic radius was calculated from $\langle D\rangle_z$, by means of the Stokes−Einstein formula

$$\langle R_H^{-1}\rangle_z^{-1} = \frac{k_B T}{6\pi\eta_0\langle D\rangle_z} \quad (6)$$

where k_B is the Boltzmann constant, T is the temperature, and η_0 is the viscosity of the solvent.

Atomic Force Microscopy (AFM). Atomic force microscopy measurements were performed in the tapping mode under ambient conditions using a commercial scanning probe microscope, Digital Instruments NanoScope dimensions 3, equipped with a Nanosensors silicon cantilever, typical spring constant 40 Nm^{-1}. Polymeric micelles were deposited on a freshly peeled out mica surface by a fast dip coating in a dilute (c ca. 5×10^{-2} g L^{-1}) $PISC_{230}$-PS_{52}-PEO_{151} aqueous solution and dried in a vacuum oven.

Cryogenic Transmission Electron Microscopy (Cryo-TEM). Cryo-TEM measurements were performed using a Zeiss EM922 EF-TEM instrument equipped with a CT3500 cryo-transfer holder (Gatan, München, Germany). Examinations were carried out at temperatures around 90 K. The transmission electron microscope was operated at an acceleration voltage of 200 kV. Zero-loss filtered images ($\Delta E = 0$ eV) were taken under reduced dose conditions (100−1000, Gatan), combined, and processed with a digital imaging processing system (Gatan Digital Micrograph 3.9 for GMS 1.4).

A drop of the terpolymer solution ($c \approx 0.1$ g L^{-1}) was put on a lacy TEM grid, where most of the liquid was removed with blotting paper, leaving a thin film stretched over the lace. The specimens were instantly vitrified by rapid immersion into liquid ethane and cooled to approximately 90 K by using liquid nitrogen in a temperature controlled freezing unit (Zeiss Cryobox, Zeiss NTS, Oberkochen, Germany). The temperature was monitored and kept constant in the chamber during all of the sample preparation steps. After freezing the specimen, was inserted into the cryo-transfer holder and transferred to the instrument.

Fluorometry. Steady-state fluorescence spectra were measured in 1 cm quartz cuvettes using a SPEX Fluorolog 3-11 fluorometer. Loading of the block terpolymer with pyrene for fluorescence measurements was done by adding 1 μL of the 5 mM stock solution of pyrene (from Aldrich, optical grade) in acetone (from Fluka, luminiscence spectroscopy grade) to 2 mL of the aqueous solution of terpolymer of various concentration. After addition of the probe, the solutions were left 24 h to equilibrate. For emission spectra, λ_{em} was 336 nm, and for excitation spectra, λ_{ex} was 382 nm.

Light Scattering Titration (LS-T) and Potentiometric Titration. Light scattering measurements during titration were performed on an ALV light scattering instrument equipped with an ALV-5000 digital correlator and 400 mW argon ion laser operated at a wavelength of 514.5 nm. A refractive index matching bath of filtered *cis*-decalin surrounded the cylindrical scattering cell, and the temperature was controlled at 25 °C using a Haake C35 termostat. LS-Ts were carried out using a Schott-Gerate computer-controlled titration setup to control sequential addition of titrant and cell stirring. The pH was measured simultaneously with a combined Ag/AgCl glass electrode calibrated with pH standards.

Results and Discussion

Characterization of $PISC_{230}$-PS_{52}-PEO_{151} Block Terpolymers. The molecular characteristics of the sample, that is, the overall molecular weight and composition, were determined by the size exclusion chromatography and by NMR spectroscopy. The results of the characterization are summarized in Table 1 and the solid state ^{13}C NMR spectra with the assigned signals are shown in Figure 1. The results clearly indicate that about 36% of isoprene units in the PISC block have not been modified. Hence, the PISC block should be regarded as a statistical copolymer of PISC and PI and has an amphiphilic rather than hydrophilic character due to the presence of hydrophobic nonfunctionalized isoprene units.

Characterization of $PISC_{230}$-PS_{52}-PEO_{151} Micelles by Light Scattering. Unlike the diblock copolymer $PISC_{132}$-PS_{113},[43] the terpolymer $PISC_{230}$-PS_{52}-PEO_{151} is directly soluble in water because (i) the PS block is relatively short and (ii) the hydrophilic PEO block further increases water solubility of the terpolymer. However, the solutions prepared by direct dissolution of the terpolymer in pure water contain irregular aggregates and undergo the transition to gel at higher polymer concentrations in a few days after preparation. The formation of gels is under investigation and will be subject of a forthcoming paper.

To prepare stable, well-defined nanoparticles, we used a procedure involving THF as a cosolvent that was finally removed by dialysis completely. Static and dynamic light scattering measurements confirmed that both mass and size of micelles prepared by this procedure (described in the Experimental Section) are well reproducible. Moreover, the nanoparticles can be transferred from acidic solutions to neutral and alkaline ones by dialysis without precipitation of the terpolymer.

The Zimm plot of static light scattering data obtained from $PISC_{230}$-PS_{52}-PEO_{151} nanoparticles in acidic media and the dynamic Zimm plot of the apparent diffusion coefficients obtained by DLS of the micelles at pH 9.2 are shown in Figure 2a and b, respectively. The concentration dependences of the scattering intensity and diffusion coefficients do not indicate any dissociation of nanoparticles within the concentration range investigated in this study. The scattering data for micelles at different solution pHs are qualitatively similar and are not shown. The typical DLS CONTIN plots (intensity weighted; the scattering angle $\theta = 90°$; $c = 2$g L^{-1}) for $PISC_{230}$-PS_{52}-PEO_{151} micelles at different solution pH (Figure 2c) show unimodal distributions of the nanoparticle size. The cumulant analysis of the DLS data yields polydispersity values ranging from 0.06 (for micelles at pH 9.2) to 0.11 (for micelles at pH 1.2). The characteristics of $PISC_{230}$-PS_{52}-PEO_{151} nanoparticles obtained by light scattering are summarized in Table 2.

The aggregation number of micelles in alkaline solution is about three times smaller than that in acidic and pure water solutions due to the increased solubility of the PISC block and decrease in amount of H-bonds between PEO and PISC in alkaline media. The measured $r = \langle S^2\rangle_z^{1/2}\langle R_H^{-1}\rangle_z$ are useful for the characterization of the particle compactness. The theoretical r value for the homogeneous hard sphere is 0.775[44] and 1.56 for the self-avoiding coil.[45] The values obtained in this study suggest that the micelles are slightly

Table 1. Characteristics of the $PISC_{230}$-PS_{52}-PEO_{151} Terpolymer Sample

composition[a]	$\langle M_{PISC}\rangle_w$[b] (kg/mol)	$\langle M_{PS}\rangle_w$[b] (kg/mol)	$\langle M_{PEO}\rangle_w$[b] (kg/mol)	PDI[c]	w[d]
$PISC_{230}$-PS_{52}-$PEO_{151}{}^{55.0}$	43.0	5.4	6.6	1.05	0.64

[a] Subscripts denote degrees of polymerization and the superscript is the overall molar mass of the terpolymer in kg/mol. [b] Molar masses of the PISC, PS and PEO blocks determined by SEC. [c] Polydispersity index determined by SEC for the precursor PI_{230}-PS_{52}-PEO_{151} terpolymer. [d] Weight fraction of modified isoprene units in PISC block, determined by solid state ^{13}C NMR spectroscopy.

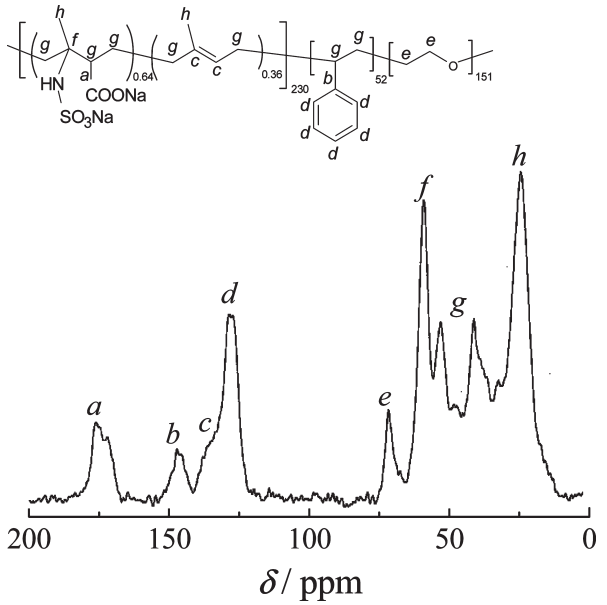

Figure 1. Solid state ^{13}C NMR spectrum of the $PISC_{230}$-PS_{52}-PEO_{151} block terpolymer.

less dense structures than hard spheres. An increase in the r value with increasing pH can be attributed to the formation of a more solvent-swollen shell structure.

Assuming that the particles have a core/shell structure and the cores are formed by polystyrene, the core radius, R_c, can be estimated using the formula

$$R_c = \left(\frac{3Z\langle M_{PS}\rangle_w}{4\pi N_A \rho_{PS}}\right)^{1/3} \quad (7)$$

where M_{PS} and ρ_{PS}, respectively, are the molar mass of the polystyrene block and the density of polystyrene. Later on we will show that apart from micelles under alkaline conditions the PISC block also resides in the core. The calculated R_c values are given in Table 2.

AFM and Cryo-TEM Imaging. To get more information on the structure of the formed nanoparticles, they were imaged (i) by AFM in the dry state, after deposition on the fresh mica surface, and (ii) by Cryo-TEM as in solution.

AFM Measurements. Despite the fact that thermodynamic conditions and forces acting on the particles at the surface differ considerably from those in the solution and that the structure can change, we have shown in our earlier studies that AFM yields valuable information on the size and size distributions of the deposited particles.[32,33,43,46] Figure 3 shows a gallery of AFM height and phase scans of $PISC_{230}$-PS_{52}-PEO_{151} micelles in acidic (Figure 3a_1 and a_2) and alkaline (Figure 3b_1 and b_2) solutions. The phase scans (Figure 3a_2 and b_2) show that the nanoparticles consist of two distinct domains (a micellar core/shell structure), which differ in viscoelastic properties.[47] The micelles are pancake-deformed, having a maximum height of about 15% of the

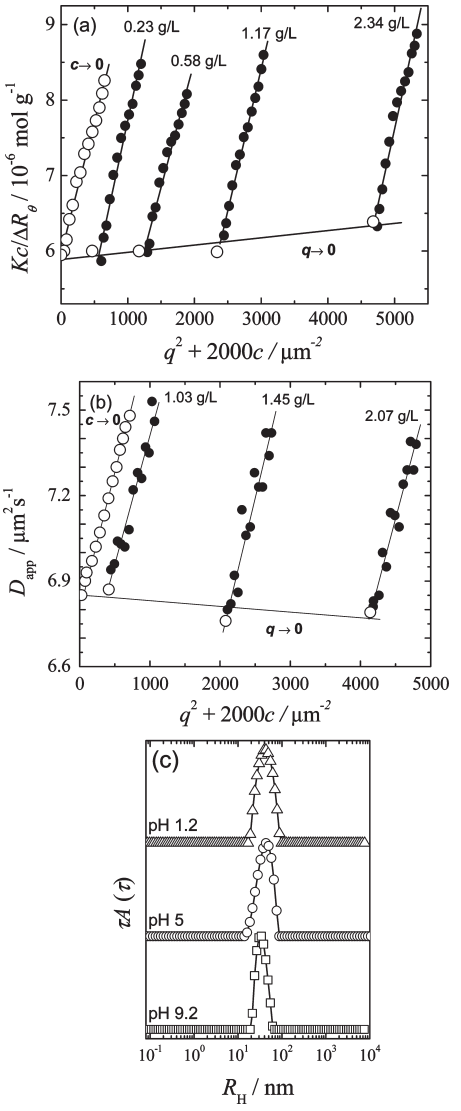

Figure 2. Results of the light scattering measurements of $PISC_{230}$-PS_{52}-PEO_{151} terpolymer solutions: (a) The Zimm plot for the acidic aqueous solutions, (b) the dynamic Zimm plot for the alkaline aqueous solutions (solid circles, experimental data; open circles, extrapolated values), and (c) DLS CONTIN plots (intensity weighted) for different solution pH measured at the scattering angle $\theta = 90°$ and $c = 2$ g L^{-1}.

maximum horizontal size, as shown in the height profile plots in Figure 4. A decrease in both horizontal and vertical size for particles in alkaline solution as compared to the particles in the acidic solution is clearly evident. Taking into account that the deposited particle volume in the dry state is roughly proportional to x^2z, where x is the diameter and z is the height,[32] we can estimate that the volume of dry $PISC_{230}$-PS_{52}-PEO_{151} micelles deposited from the acidic solution is about 60 times larger than that of the alkaline solution micelles. With respect to the molar mass ratio, which is only about 3, such a big difference cannot be explained only as a result of different particle densities. Instead, it suggests that,

Table 2. Characteristics of $PISC_{230}$-PS_{52}-PEO_{151} Micelles

sample	0.1 M HCl, pH 1.2	H_2O, pH 5.0	0.05 M $Na_2B_4O_7$, pH 9.2
dn/dc, mL/g[a]	0.165	0.171	0.176
$\langle M\rangle_w \times 10^{-6}$, g/mol[b]	16.8	17.9	6.2
$\langle S^2\rangle_z^{1/2}$, nm[b]	42	43	31
$\langle R_H^{-1}\rangle_z^{-1}$, nm[c]	46	47	32
Z[d]	305	325	113
r[e]	0.91	0.91	0.97
R_c, nm[f]	9[g] (16[h])	10[g] (18[h])	6[g] (4[i])
$P \times 10^{-5}$[j]	2.4	1.9	1.8
cmc, mg/L[j]			20

[a] $PISC_{230}$-PS_{52}-PEO_{151} refractive index increments calculated as mass averages of the homopolymer values. [b] Molar mass and gyration radius, by SLS. [c] Hydrodynamic radius, by DLS. [d] Aggregation number, $Z = \langle M\rangle_w/\langle M_{cop}\rangle_w$. [e] Gyration radius to hydrodynamic radius ratio, $r = \langle S^2\rangle_z^{1/2}\langle R_H^{-1}\rangle_z$. [f] Core radius. [g] Core radius calculated from Z by eq 7. [h] Core radius calculated from Z by eq 7 and measured by Cryo-TEM. [i] Core radius calculated from Z by eq 7 and measured by AFM. [j] Partition coefficient of pyrene between micelles and bulk solution, and critical micelle concentration, by pyrene emission spectra measurement.

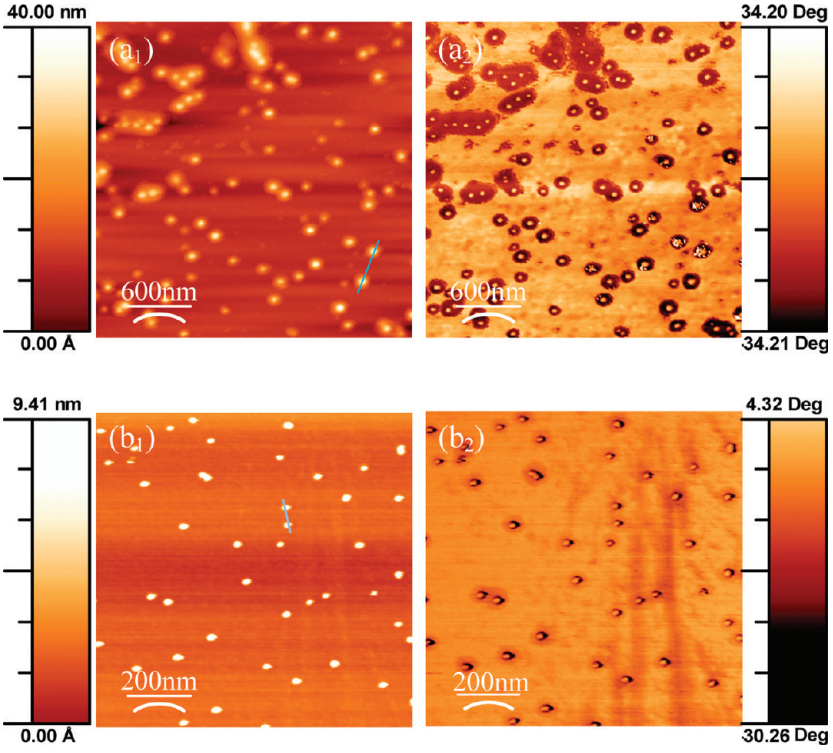

Figure 3. AFM scans (top view) of the $PISC_{230}$-PS_{52}-PEO_{151} micelles deposited from (a) acidic (3 × 3 μm) and (b) alkaline (1 × 1 μm) solution: (1) height, (2) phase. Lines indicate horizontal tip motions corresponding to section analysis shown in Figure 4.

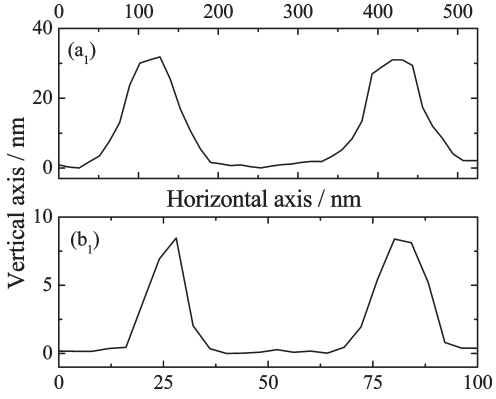

Figure 4. Section analysis of the AFM scans shown in Figure $3a_1$ and b_1.

in the case of the alkaline solution micelles, only the small PS core is detected by the AFM tip, while the imaged core of the acidic solution micelles consists of both PS and PISC domains. That is why the apparent PS core radii of the acidic solution micelles calculated by eq 7 are lower than those estimated as $z/2$, while for the alkaline solution micelles, $R_c > z/2$. Here we must point out that, although the particle heights measured by AFM are widely used for the estimation of the core radius, only sufficiently large cores (several tens of nm) do not deform after deposition so that the maximum vertical distance obtained from the AFM scan compares well with the actual core diameter.[33] Small cores are more mobile and one cannot preclude their deformation after deposition on the mica surface. Hence, the core radius obtained by measuring the maximum vertical distances, $z/2 = 4$ nm, is slightly smaller than that estimated from the aggregation number ($R_c = 6$ nm).

Cryo-TEM Measurements. Cryo-TEM of the acidic solution micelles (Figure 5a) revealed the raspberry-like cores with the radius of about 16 nm. This value is in accordance with the AFM results and indicates that the nanoparticles are stable, hard, and do not change significantly upon deposition on mica surface. Cryo-TEM thus confirms that the acidic solution micelles have cores with a more complex morphology. The images of $PISC_{230}$-PS_{52}-PEO_{151}

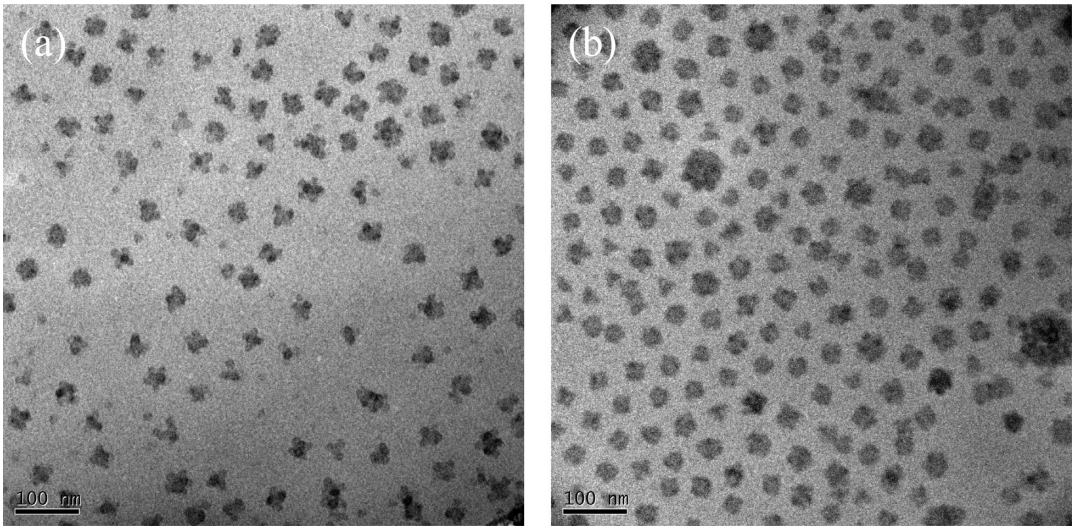

Figure 5. Cryo-TEM images of the $PISC_{230}$-PS_{52}-PEO_{151} micelles deposited from (a) acidic solution and (b) pure water. Scale bars indicate 100 nm.

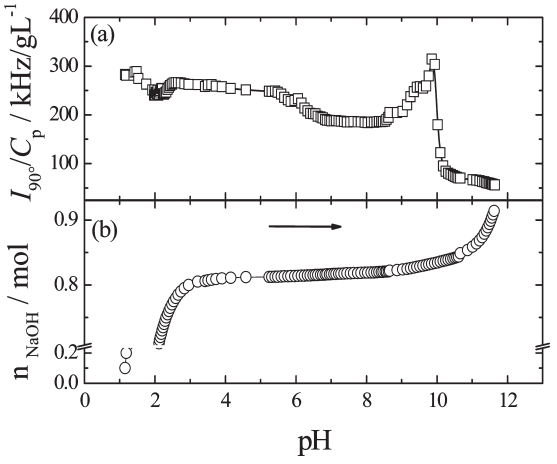

Figure 6. (a) $I_{90°}/C_p$ as a function of pH for an aqueous solution of $PISC_{230}$-PS_{52}-PEO_{151} at 0.1 M HCl, C_p = 1.0 g L^{-1}. The arrow indicates the direction of the pH scan. (b) alkalimetric titration of $PISC_{230}$-PS_{52}-PEO_{151} solution in 0.1 M HCl by 1 M NaOH.

nanoparticles contain from two to five dark spots, which correspond to dense domains formed by the collapsed PS blocks, embedded in a looser medium of partially water-swollen, entangled PISC blocks. The PEO blocks are in good solvent condition and form the micelle shell. After dialysis against pure water, the raspberry-like core of the micelles prepared in 0.1 M HCl reorganizes and forms more spherical structures. The size distribution becomes narrower with only slight changes in the mean value and the PS domains (the dark spots) are still visible in the Cryo-TEM image in Figure 5b. The transition is connected with the swelling of the PISC chains due to both a pH and ionic strength effects. The carboxyl groups become charged (more repulsions along the PISC chains) and ionic strength decreases (less charge screening), which induced swelling of PISC block and allows for a better accommodation of PS domains in the core.

Potentiometric and Light Scattering Titration (LS-T). To study the transition from acidic solution micelles to those found in alkaline solution, we carried out the light scattering (LS-T) and potentiometric titration experiment. The titration curves are shown in Figure 6a and b, respectively. As we reported recently,[43] the neutralization of COOH and $NH_2{}^+SO_3{}^-$ groups in the shell of PS-PISC nanoparticles in acidic solution is slow due to the slow diffusion of OH^- ions into the dense, collapsed PISC shell, occurring on the time scale of hours. Therefore, one has to keep in mind that the LS-T curve corresponds to a not fully equilibrated system.

Figure 6a shows that the increase in the solution pH above 8.3 leads to pronounced changes in light scattering intensity that are related to the deprotonation of nitrogen in sulfamate groups: Once the negative charge of both the carboxylate and the sulfamate groups is not compensated, $PISC_{230}$-PS_{52}-PEO_{151} nanoparticles swell due to increased electrostatic repulsion between the PISC chains and scattering intensity increases. Later, as the swollen nanoparticles dissociate, the scattering intensity steeply decreases below the value it had before the solution reached pH 8.3. The peak in the LS-T curve at pH 10 thus belongs to a nonequilibrium, transition state between that of nanoparticles with multicompartment cores and micelles with a mixed shell. This transition is irreversible, acidification of the small micelles (back-titration, data not shown) showed qualitatively different aggregation behavior. Finally, in acidic solution polydisperse, ill-defined aggregates are formed and precipitate after some time. Thus, it appears that the strong hydrogen-bonding interaction between the PEO and the PISC mixed blocks and high ionic strength plays the key role in such behavior.

^{1}H NMR Spectroscopy. Besides the basic characterization of the sample, NMR spectroscopy yields information on intermolecular interactions between polymer chains and their dynamics in the nanoparticles. The ^{1}H NMR spectra of the $PISC_{230}$-PS_{52}-PEO_{151} solutions in dimethyl sulfoxide-d_6 (curve 1), 0.01 M DCl in D_2O (curve 2), and 0.01 M NaOD in D_2O (curve 3) are shown in Figure 7. Signals of aromatic protons of the PS block in the region from about 6.5 to 8.5 ppm are suppressed in aqueous solutions due to immobility of PS domains of the nanoparticles. All signals assigned to polymer protons are broad due to the restricted mobility of $PISC_{230}$-PS_{52}-PEO_{151} chains in the nanoparticles. The other intensive and narrow signals correspond to residual protons of water and THF and to silicon grease. The CH_2O signals of the PEO block (Insert in Figure 7) are narrow in all three samples, reflecting that PEO chain motions are not restricted by intermolecular interactions. The downfield shift in aqueous solutions is caused by the deshielding effect of weak $HCH\cdots OH_2$ hydrogen bonds.[48] The acidic solution exhibits an additional, broad signal at 3.85 ppm which can be ascribed to the formation of a hydrogen bond stabilized

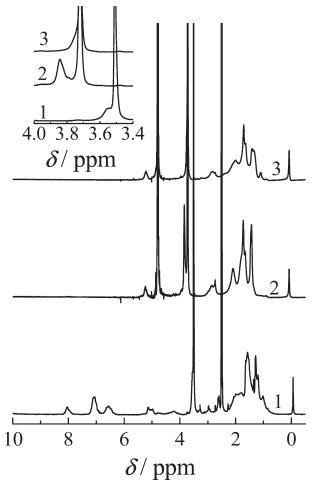

Figure 7. ^{1}H NMR spectra of $PISC_{230}$-PS_{52}-PEO_{151} solutions in dimethyl sulfoxide-d_6 (curve 1), 0.01 M DCl in D_2O (curve 2), and 0.01 M NaOD in D_2O (curve 3).

complex between PEO and PISC at the core/shell interface of the micelles. However, even in the acidic solution, the majority of PEO segments are well segregated from the core-forming PISC.

Fluorescence Spectroscopy. Steady-state fluorescence spectroscopy with pyrene as a hydrophobic fluorescence probe has been used for the determination of (i) the critical micelle concentration of the $PISC_{230}$-PS_{52}-PEO_{151} terpolymer in aqueous solution at different pH (see Supporting Information for more details and different possibilities to determine cmc) and (ii) the partition coefficient of pyrene between the micelles and the aqueous phase. To estimate the true values of cmc corresponding to the onset of formation of the multimolecular micelles in these systems, we employed the methods reported by Astafieva et al.[49] and Wilhelm et al.[50] and further used by many others.[51−53] The ratio of the pyrene molar amounts in the aqueous and in the micellar phase, n_m/n_w, can be expressed as a function of the I_1 as

$$\frac{n_m}{n_w} = \frac{I_1 - (I_1)_{min}}{(I_1)_{max} - I_1} \quad (8)$$

where the indices min and max, respectively, denote the limiting I_1 values for pyrene in water and in the micellar microphase.

The fluorescence data can be further used for the determination of the partition coefficient of pyrene between the bulk solution and the micelles[49−53]

$$P = \frac{n_m V_w}{n_w V_m} = \frac{n_m \rho_{PS}}{n_w w_{PS}(c - \text{cmc})} \quad (9)$$

where c is the mass concentration of the terpolymer in the solution, cmc is the critical micelle concentration of the terpolymer, n_m and n_w, respectively, are the pyrene molar amounts in the micellar microphase and in the aqueous phase, V_m and V_w are the volumes of the two phases, ρ_{PS} is the density of the polystyrene core, and w_{PS} is the polystyrene weight-fraction in the terpolymer.

Assuming that the PS density in the core is the same as in bulk polystyrene, ρ_{PS} = 1.04 g/mL, the partition coefficient of pyrene between the aqueous and polystyrene phases above cmc can by calculated from the slope of the n_m/n_w versus c plot (Figure 8). The low but finite value of n_m/n_w below cmc (20 mg L^{-1}) shows that the pyrene associates with $PISC_{230}$-

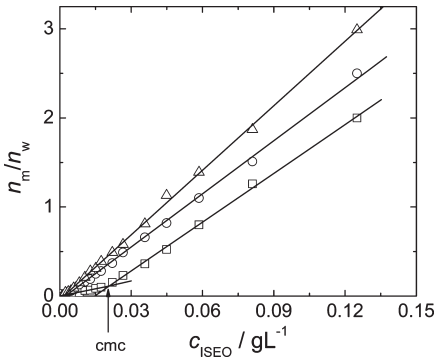

Figure 8. Plot of n_m/n_w vs the $PISC_{230}$-PS_{52}-PEO_{151} block terpolymer concentration: (□) pH 9.2; (○) pH 5; (△) pH 1.2.

Scheme 2. Morphologies of $PISC_{230}$-PS_{52}-PEO_{151} Micelles at Different pHs

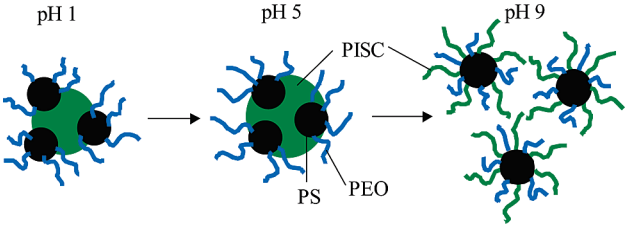

PS_{52}-PEO_{151} unimers or premicellar aggregates only in alkaline solution. The cmc for micelles in 0.1 M HCl and pure water were not detected which suggests that the micellar core formed by PS and PISC is a kinetically trapped structure. The values of the partition coefficient are summarized in Table 2. They decrease with increasing pH due to the decreasing hydrophobicity of the PISC domain but the decrease is small because pyrene is mostly solubilized in the PS domain.

Morphology of $PISC_{230}$-PS_{52}-PEO_{151} Micelles in Acidic and Alkaline Solution. The obtained experimental data allows us to propose a model of the $PISC_{230}$-PS_{52}-PEO_{151} micelle morphology in both acidic and alkaline solution. The polyelectrolyte PISC block plays the key role in the structure of the terpolymer assemblies. In acidic solution, both PISC carboxylic and sulfamate groups are protonated. The positive and negative charge in the $NH_2^+SO_3^-$ groups mutually compensates and the PISC block is neutral and fairly hydrophobic due to the presence of unmodified isoprene units in the chain. Therefore, the PISC blocks aggregate into a partly collapsed, only slightly solvated, micellar core containing domains formed by the middle PS blocks and surrounded by a PEO shell (Scheme 2). ^{1}H NMR measurements show that PEO and PISC chains are partially intermixed in the core/shell interfacial region and form an interpolymer complex. A raspberry-like structure of the core with compact PS domains (smaller cores) was found by Cryo-TEM.

Cryo-TEM imaging also revealed that when the solution pH is increased to less acidic values of about 5 (dialysis against pure water), the raspberry-like core of micelles prepared in 0.1 M HCl undergoes a transition to a more spherical structure. Light scattering measurements showed that the transition is accompanied by a slight change in the size of the micelles (shown in Table 2). The changes are caused by increased solubility of the PISC block due to ionization of carboxylic groups above pH 4. The core of the micelles consisting of the PS and PISC domains slightly swells because PISC becomes more hydrophilic. The swollen PISC core with more loosely packed chains allows for a

better spatial incorporation of PS domains and the raspberry-like structure is less visible.

In the alkaline region (dialysis against 0.05 M $Na_2B_4O_7$), the PISC blocks with fully ionized carboxyl groups and deprotonated NH groups become more hydrophilic and the micelles dissociate to particles with ca. three times lower molar mass. The original PS domains become the cores of the smaller micelles after the dissolution of PISC in which they were embedded. The PS core is surrounded by the mixed shell formed by both PEO and PISC blocks. Due to the stretching of PISC chains, the small micelles are less compact as evidenced by the increased ratio of the gyration radius to the hydrodynamic radius as compared to micelles in the acidic solution. Because the PS core is very small, the micelles are no longer in a kinetically trapped state and the alkaline solution micelles have a cmc measurable by the fluorescence probe technique.

Conclusions

It was found that the multifunctional block terpolymer $PISC_{230}$-PS_{52}-PEO_{151}, prepared from the precursor block terpolymer polyisoprene-*block*-polystyrene-*block*-poly(ethylene oxide), forms nanoparticles when dissolved in acidic aqueous media using tetrahydrofuran as a cosolvent that is then removed by dialysis after the dissolution of the sample.

Cryo-TEM images of the acidic aqueous solution revealed that the terpolymer self-assembles into multicompartment micelles with a PEO shell and a raspberry-like PISC core containing PS domains (Scheme 2). These multicompartment micelles are in a kinetically trapped state in acidic media. If the solution pH is increased to the alkaline region, the solubility of the PISC increases due to (i) ionization of carboxylic groups and (ii) deprotonation of $NH_2{}^+SO_3{}^-$ groups, which results in dissociation of multicompartment micelles into smaller assemblies with a PS core and a mixed shell of PISC and PEO (Scheme 2). The latter are not kinetically frozen, having a cmc measurable by the fluorescence probe technique.

Although the PISC block contains strong electrolyte $SO_3{}^-$ groups, its water solubility is reduced by charge compensation within the PISC block and H-bonding with PEO block. Furthermore, the presence of unmodified isoprene units (36 wt %) giving the PISC blocks an amphiphilic character and contributing to its aggregation in acidic solution. Even though the PISC core of the multicompartment micelles is kinetically trapped in aqueous solution, it can be easily disrupted at elevated pH as a result of the increased charge density onto the PISC chains and subsequent absence of H-bonding between PEO and PISC blocks.

Acknowledgment. The authors thank the Marie Curie Research and Training Network (Grant No. 505 027, POLYAMPHI) for the financial support. S.P. and K.P. acknowledge financial support from the Greek-Czech Bilateral Grant (Greek GSRT Grant No. 191-γ/2005). K.P. also acknowledges the financial support from the Ministry of Education of the Czech Republic (Long-Term Research Project No. MSM0021620857) and the Grant Agency of the Czech Republic (Grant No. 203/07/0659) and Grant Agency of the Academy of Science of the Czech Republic (Grant No. IAA401110702). M.U. thanks Dr. Milena Špírková from the Institute of Macromolecular Chemistry of the Academy of Science of the Czech Republic for the assistance with AFM measurements.

Supporting Information Available: Determination of critical micelle concentration (cmc) from excitation spectra and I_1/I_3 ratios of pyrene fluorescence at different solution pH. This material is available free of charge via the Internet at http://pubs.acs.org.

References and Notes

(1) Forster, S.; Abetz, V.; Müller, A. H. E. *Adv. Polym. Sci.* **2004**, *166*, 173.
(2) Rodriguez-Hernandez, J.; Checot, F.; Gnanou, Y.; Lecommandoux, S. *Prog. Polym. Sci.* **2005**, *30*, 691.
(3) Fustin, C. A.; Abetz, V.; Gohy, J. F. *Eur. Phys. J. E* **2005**, *16*, 291.
(4) Hadjichristidis, N., Pispas, S., Floudas, G., Eds. *Block copolymers. Synthetic strategies, physical properties and applications*; Wiley-Interscience: New York, 2002.
(5) Laschewsky, A. *Curr. Opin. Colloid Interface Sci.* **2003**, *8*, 274.
(6) Lutz, J. F.; Laschewsky, A. *Macromol. Chem. Phys.* **2005**, *206*, 813.
(7) Kubowicz, S.; Baussard, J. F.; Lutz, J. F.; Thünemann, A. F.; von Berlepsch, H.; Laschewsky, A. *Angew. Chem., Int. Ed.* **2005**, *44*, 5262.
(8) Walther, A.; Millard, P.; Goldmann, A.; Lovestead, T.; Schacher, F.; Barner-Kowollik, C.; Müller, A. H. E. *Macromolecules* **2008**, *41*, 8608.
(9) Zhu, J.; Jiang, W. *Macromolecules* **2005**, *38*, 9315.
(10) Njikang, G.; Han, D.; Wang, J.; Liu, G. *Macromolecules* **2008**, *41*, 9727.
(11) Cheng, L.; Hou, G.; Miao, J.; Chen, D.; Jiang, M.; Zhu, L. *Macromolecules* **2008**, *41*, 8159.
(12) Schacher, F.; Walther, A.; Ruppel, M.; Müller, A. H. E. *Polym. Mater. Sci. Eng.* **2007**, *96*, 94.
(13) Li, Z.; Kesselman, E.; Talmon, Y.; Hillmyer, M. A.; Lodge, T. P. *Science* **2004**, *306*, 98.
(14) Saito, N.; Liu, Ch.; Lodge, T. P.; Hillmyer, M. A. *Macromolecules* **2008**, *41*, 8815.
(15) Liu, Ch.; Hillmyer, M. A.; Lodge, T. P. *Langmuir* **2008**, *24*, 12001.
(16) Brannan, A. K.; Bates, F. S. *Macromolecules* **2004**, *37*, 8816.
(17) Thünemann, A. F.; Kubowicz, S.; von Berlepsch, H.; Mohwald, H. *Langmuir* **2006**, *22*, 2506.
(18) Hu, J.; Liu, G. *Macromolecules* **2005**, *38*, 8058.
(19) Yan, X.; Liu, G.; Hu, J.; Willson, C. G. *Macromolecules* **2006**, *39*, 1906.
(20) Zhu, J.; Hayward, R. C. *Macromolecules* **2008**, *41*, 7794.
(21) Cui, H. G.; Chen, Z. Y.; Zhong, S.; Wooley, K. L.; Pochan, D. J. *Science* **2007**, *317*, 647.
(22) Li, Z. B.; Hillmyer, M. A.; Lodge, T. P. *Macromolecules* **2006**, *39*, 765.
(23) Gromadzki, D.; Filïppov, S.; Netopilík, M.; Makuška, R.; Jigounov, A.; Pleštil, J.; Horský, J.; Štěpánek, P. *Eur. Polym. J.* **2009**, *45*, 1748.
(24) Ostmark, E.; Nystrom, D.; Malmstrom, E. *Macromolecules* **2008**, *41*, 4405.
(25) Xiong, D.; Shi, L.; Jiang, X.; An, Y.; Chen, X.; Lü, J. *Macromol. Rapid Commun.* **2007**, *28*, 194.
(26) Cai, Y.; Armes, S. P. *Macromolecules* **2004**, *37*, 7116.
(27) Matějíček, P.; Uchman, M.; Lokajova, J.; Štěpánek, M.; Procházka, K.; Špírková, M. *J. Phys. Chem. B* **2007**, *111*, 8394.
(28) Štěpánek, M.; Podhájecká, K.; Tesařová, E.; Procházka, K.; Tuzar, Z.; Brown, W. *Langmuir* **2001**, *17*, 4240.
(29) Voets, I. K.; Fokkin, R.; Hellweg, T.; King, S. M.; de Waard, P.; de Keizer, A.; Stuart, M. A. C. *Soft Matter* **2009**, *5*, 999.
(30) Procházka, K.; Martin, T. J.; Webber, S. E.; Munk, P. *Macromolecules* **1996**, *29*, 6526.
(31) Talingting, M. R.; Munk, P.; Webber, S. E.; Tuzar, Z. *Macromolecules* **1999**, *32*, 1593.
(32) Matějíček, P.; Štěpánek, M.; Uchman, M.; Procházka, K.; Špírková, M. *Collect. Czech. Chem. Commun.* **2006**, *71*, 723.
(33) Štěpánek, M.; Humpolíčková, J.; Procházka, K.; Hof, M.; Tuzar, Z.; Špírková, M.; Wolff, T. *Collect. Czech. Chem. Commun.* **2003**, *68*, 2120.
(34) Zhong, S.; Cui, H. G.; Chen, Z. Y.; Wooley, K. L.; Pochan, D. J. *Soft Matter* **2008**, *4*, 90.
(35) Harrisson, S.; Wooley, K. L. *Chem. Commun.* **2005**, *26*, 3259.
(36) Chen, Z. Y.; Ciu, H. G.; Hales, K.; Li, Z. B.; Qi, K; Pochan, D. J.; Wooley, K. L. *J. Am. Chem. Soc.* **2005**, *127*, 8592.
(37) Walther, A.; Müller, A. H. E. *Soft Matter* **2008**, *4*, 663.
(38) Gohy, J. F.; Khousakoun, E.; Willet, N.; Varshney, S. K.; Jerome, R. *Macromol. Rapid Commun.* **2004**, *25*, 1536.
(39) Pispas, S. *J. Polym. Sci., Part A: Polym. Chem.* **2006**, *44*, 606.
(40) Cox, M. M.; Nelson, D. L. *Lehninger Principles of Biochemistry*; W.H. Freeman: New York, 2004; pp 1100.

(41) Hadjichrisitidis, N.; Iatrou, H.; Pispas, S.; Pitsikalis, M. *J. Polym. Sci., Part A: Polym. Chem.* **2000**, *38*, 3211.
(42) *Polymer Handbook*, 3rd ed.; Brandup, J., Immergut, E. H., Eds.; Wiley-Interscience: New York, 1989; Vol. VII, pp 409−484.
(43) Uchman, M.; Procházka, K.; Štěpánek, M.; Mountrichas, G.; Pispas, S.; Špírková, M.; Walther, A. *Langmuir* **2007**, *24*, 12017.
(44) Pyun, C. W.; Fixman, M. *J. Chem. Phys.* **1965**, *42*, 3838.
(45) Oono, Y. *J. Chem. Phys.* **1983**, *79*, 4629.
(46) Matějíček, P.; Humpolíčková, J.; Procházka, K.; Tuzar, Z.; Špírková, M.; Hof, M.; Webber, S. E. *J. Phys. Chem. B* **2003**, *107*, 8232.
(47) Liu, D.; Wang, T.; Keddie, J. L. *Langmuir* **2009**, *25*, 4526–4534.
(48) Mizuno, K.; Imafuji, S.; Fujiwara, T.; Ohta, T.; Tamiya, Y. *J. Phys. Chem. B* **2003**, *107*, 3972.
(49) Astafieva, I.; Zhong, X. F.; Eisenberg, E. *Macromolecules* **1993**, *26*, 7339.
(50) Wilhelm, M.; Zhao, C. L.; Wang, Y.; Xu, R.; Winnik, M. A. *Macromolecules* **1991**, *24*, 1033.
(51) Lysenko, E. A.; Bronich, T. K.; Slonkina, E. V.; Eisenberg, E.; Kabanov, V. A.; Kabanov, A. V. *Macromolecules* **2002**, *35*, 6351.
(52) Szczubialka, K.; Ishikawa, K.; Morishima, Y. *Langmuir* **1999**, *15*, 454.
(53) Štěpánek, M.; Krijtová, K.; Procházka, K.; Teng, Y.; Webber, S. E.; Munk, P. *Acta Polym.* **1998**, *49*, 96.